JCTC Journal of Chemical Theory and Computation

Article

pubs.acs.org/JCTC

# Migration of Holstein Polarons in Anatase $TiO_2$

Likai Yan[†,‡] and Hanning Chen*[,‡]

[†]Department of Chemistry, Northeast Normal University, 5268 Renmin Street, Changchun 130024, People's Republic of China

[‡]Department of Chemistry, The George Washington University, 725 21st Street, NW, Washington, DC 20052, United States

Supporting Information

**ABSTRACT:** A simple yet reliable valence bond theory was applied to ascertain the effective size and shape for the electron and hole polarons in bulk anatase $TiO_2$ by examining the extent of polaron charge delocalization. It was found that the electron polaron is approximately 2 times as large as its hole counterpart, leading to a faster electron diffusion than hole hopping with regard to the electron−phonon coupling strength. Moreover, the oblate hole polaron exhibits a pronounced directional heterogeneity in migration, whereas the nearly spherical electron polaron tends to diffuse along all possible lattice directions. In light of the notable delocalization characteristics of both polarons, their migration should proceed in an adiabatic manner, and their rates can be calculated by the Arrhenius equation. It turns out that our calculated polaron mobilities at 300 and 1300K are both in excellent agreement with experimental values, justifying our novel approach for Holstein polaron modeling in crystalline semiconductors.

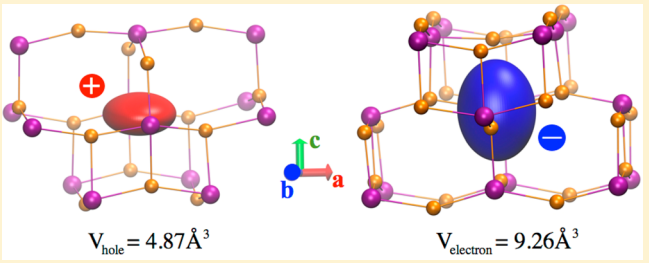


## 1. INTRODUCTION

Titanium dioxide, $TiO_2$, is one of the most widely used semiconductors in industry thanks to its extraordinary chemical stability,[1] superior electronic property,[2] and high natural abundance. In ambient conditions, a $TiO_2$ pigment is a white solid substance with excellent light scattering efficiency[3] that can be exploited in antireflection coating[4] and even in preventative skin care[5] because of its lack of toxicity. By contrast, a nanoscale thin film of $TiO_2$ appears transparent under sunlight,[6] because it only absorbs ultraviolet light with an optical band gap of ∼3.2 eV.[7] In fact, the world's first photocatalytic water-splitting experiment[8] was carried out by A. Fujishima and K. Honda in 1972 on a $TiO_2$ electrode, which was subject to ultraviolet irradiation. Over the last 40 years, numerous efforts have been invested to improve the solar energy conversion efficiency of $TiO_2$-based materials, aiming to tackle the impending global energy challenge.[9] For instance, a carbon-doped $TiO_2$ nanotube array[10] with high aspect ratio has achieved an impressive 20-fold amplification of the photocurrent in the visible region (>420 nm) that can be ascribed to the reduced band gap and high surface area. In another study,[11] an enormous 66 times enhancement on photocurrent was also observed on anodic $TiO_2$ when the incident wavelength was 633 nm, and this wavelength also evoked the plasmon resonance of the Au nanoparticles, which were deposited on the $TiO_2$ film. More recently, a biomimetic $TiO_2$ anode templated by cellulose nanofiber[12] further improved the yields of hydrogen production by taking advantage of the longer optical path and faster charge transport of the capillary architecture.

In a complete water-splitting cycle, an electron−hole pair is first generated upon light absorption before the dissociated electron and hole migrate to two opposite electrodes to reduce hydrated protons and to oxidize water molecules, respectively. Apparently, the charge migration in $TiO_2$ is a key process that not only prefers high mobility but also requires controllable direction. For instance, three surfaces of anatase $TiO_2$, namely, [100], [101], and [001], exhibit distinctly different photocatalytic efficiencies,[13] which are conjectured to arise from the notable disparity on charge migration rate among the three lattice directions in single-crystalline anatase.[14] Interestingly, an n-type anatase $TiO_2$ film can be even reversed to p-type with an adsorbed water layer as examined by surface photovoltage (SPV) and infrared (IR) spectra,[15] suggesting the importance of controlling the relative migration capacity between electrons and holes under various conditions to meet our desired needs. Certainly, a precise modulation of the charge migration in $TiO_2$ using a rich library of now available experimental techniques[16] is not an easy task because it demands a thorough understanding of the migration mechanism down to the atomistic level. Surprisingly, in spite of many pioneering investigations,[14,17] the charge migration mechanism is still elusive to date even for the pristine (undoped) $TiO_2$ polymorphs, and it continues to draw attention from both experimental and theoretical sides.[18] For example, a Marcus's two-state model based on environmental reorganization[19] has been proposed to examine the site-to-site hopping of small polarons.[20]

By far, the most widely used methodology to investigate small polaron migration is the Emin−Holstein−Austin−Mott (EHAM) theory,[21] which has evolved into several variants

**Received:** July 11, 2014
**Published:** September 30, 2014





dx.doi.org/10.1021/ct500873s | J. Chem. Theory Comput. 2014, 10, 4995−5001

based on different ab initio levels of theory. As an example, in a DFT+$U$ study[14a] on electron transport in bulk $TiO_2$, an effective $U$ parameter of 10 eV was introduced to localize an electron on Ti 3d orbitals before the evaluation of the polaron activation energy. Although the DFT+$U$ method is computationally efficient, it is nearly impossible to have a universal $U$ parameter that will match every physical property of a given system because electrons may have distinct overdelocalization tendencies due to the self-interaction errors[22] in DFT. A plausible alternative to DFT+$U$ is the complete active electronic self-consistent-field (CASSCF) method wherein the system's wave function is represented as a linear combination of high-spin and low-spin states, yielding accurately determined electronic coupling strength. For electron polaron transfer in chromia ($\alpha$-$Cr_2O_3$), the electronic coupling in its high-spin state was found to be significantly stronger than that in its low-spin state.[23] By contrast, the two spin states have equally strong coupling strength for hole polaron transfer.[23] Although the CASSCF method can be extended to periodic systems through reformulation of Bloch states to Wannier functions[24] by capturing the predominantly local character of electron correlation effects, its computational cost is prohibitively high for defective supercells, which must be large enough to alleviate boundary effects due to crystalline distortion. In a recent study,[20] the unrestricted Hartree−Fock and hybrid DFT functionals were also employed to explore the reaction path of polaron transfer in bulk $CeO_2$, both confirming the previously proposed adiabatic hopping mechanism.[25] For a complete discussion on the theoretical prediction of polaron mobility in crystalline materials, please refer to an earlier review article.[19] Aiming to explicitly construct a polaron in consideration of its charge delocalization over lattice sites, we will present a novel modeling approach inspired by both the valence bond theory[26] and constrained density functional theory.[27]

## 2. SIMULATION METHODS AND RESULTS

According to the Holstein theory,[28] a moving charged particle in a polarizable condensed phase can be considered as a quasiparticle called polaron,[29] which consists of the charge carrier and its surrounding phonon cloud. For example, in the presence of an excess electron, the crystal lattice of $TiO_2$ will undergo appreciable deformation to effectively screen the electronic charge through electron−phonon (EP) coupling.[30] With regard to the short-range characteristics of the EP coupling in most semiconductors,[31] the polaron migration in crystalline substance is often described by the tight-binding Holstein Hamiltonian:[32]

$$\hat{H} = -J\sum_i \sum_j c_i^\dagger c_j + \hbar\omega_0 \sum_i b_i^\dagger b_i - \lambda \sum_i (b_i^\dagger + b_i) c_i^\dagger c_i \quad (1)$$

where $c_i^\dagger(c_i)$ and $b_i^\dagger(b_i)$ are, respectively, the creation (annihilation) operators for electrons and photons on the $i$ th polaron site, $J$ is the intersite hopping integral, $\omega_0$ is the photon angular frequency, and $\lambda$ is the reorganization energy that reflects the EP coupling strength. In the weak EP coupling limit ($\lambda \ll \hbar\omega_0$), the photogenrated polaron behaves like a soliton, a continuously propagating wave with a well-maintained shape. By contrast, a strong EP coupling ($\lambda \gg \hbar\omega_0$) results in notable charge localization on very few lattice sites that may significantly impede polaron migration with a heavier effective mass. Moreover, the detailed polaron migration mechanism is also governed by the so-called adiabaticity ratio $\alpha = (\hbar\omega_0/J)$. If $\alpha \ll 1$ wherein the molecular vibration is always outpaced by charge hopping, the polaron migration should proceed along the adiabatic potential surface, and its rate, $k_p$, is given by the Arrhenius equation:[33]

$$k_p = \frac{\omega_0}{2\pi} e^{-\Delta G^*/k_B T} \quad (2)$$

where $\Delta G^*$ is the adiabatic activation energy. In the diabatic limit $\alpha \gg 1$, the Marcus theory[34] has to be adopted to account for the recrossing of dividing surface[35] due to feeble electronic coupling. Although the Holstein Hamiltonian usually works quite well on one-dimensional model systems,[36] its extension to three-dimensional realistic crystals turns out to be nontrivial. The challenge primarily lies on the rapidly growing nonlocal EP coupling terms,[37] referred to as the Peierls coupling,[38] whenever a new dimension is added. Moreover, the definition of a polaron site becomes fairly vague in high-dimensional systems as it may vary drastically from a single atom[39] to several unit cells[18c] depending on the EP coupling strength. In order to address all these issues, we will apply a seemly intuitive, but rather reliable, valence-bond (VB) approach to effectively incorporate EP coupling into adiabatic quantum chemistry calculations. Because anatase is more photochemically active than rutile,[40] another naturally occurring $TiO_2$ polymorph, we will focus our following discussions on bulk anatase, which is represented by a 5 × 5 × 2 super cell with a total of 600 atoms. Moreover, as shown by our partial density of states (PDOS) calculations (Figure 1), the valence holes tend to reside in the $p$

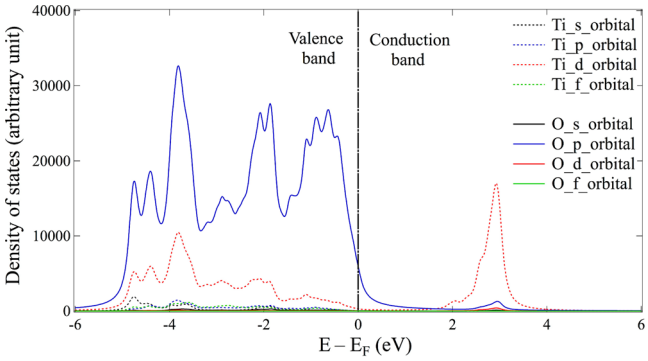


**Figure 1.** Calculated partial density of states for bulk anatase $TiO_2$. $E_F$ is the Fermi energy.

orbitals of oxygen atoms while the conduction electrons are found to occupy the d orbitals of titanium atoms. Therefore, the hole (electron) migration can be regarded as a charge transfer process between oxygen (titanium) atoms. In our simulations, a hole polaron is created by removing an electron from the super cell, whereas an electron polaron is formed after the addition of an excess electron. Unless otherwise specified, all simulations were performed using CP2K software[41] with the Goedecker−Teter−Hutter (GTH) pseudopotential,[42] Perdew−Burke−Ernzehof (PBE) exchange−correlation functional[43] and polarized−valence−double-$\zeta$ (PVDZ) basis set.[44]

In our VB approach, a polaron $\Psi = \Sigma_i c_i \varphi_i$ is formulated as a linear combination of some single-site charged complexes (abbreviated as complex thereafter), $\varphi$, each of which consists of a pivotal atom and all of its adjacent atoms that are directly connected by chemical bonds. Specifically, a hole complex includes a pivotal oxygen atom and its three coordinated


dx.doi.org/10.1021/ct500873s | J. Chem. Theory Comput. 2014, 10, 4995−5001

titanium atoms (Figure 2a), whereas an electron complex is comprised of a pivotal titanium atom and six coordinated

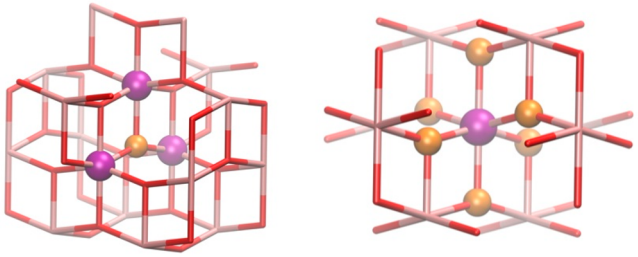

(a) hole complex (b) electron complex

**Figure 2.** Hole (a) and electron (b) single-site complexes in anatase $TiO_2$. The constituent oxygen and titanium atoms are modeled as orange and purple spheres, respectively.

oxygen atoms (Figure 2b). Accordingly, a complex's charge, $Q_C$, can be defined as $Q_C = Q_P + (1/N_C)(\Sigma_{i=1}^{N_C} Q_i)$, where $N_C$ is the coordination number, $Q_P$ is the charge of the pivotal atom, and $Q_i$ is the charge of its $i$ th coordinated atom. In the present study, the constrained density functional theory (CDFT)[27] was applied to impose the density derived atomic point charge (DDAPC)[45] constraints of $Q_{hole} = +1$ and $Q_{electron} = -1$ to the hole and electron complexes, respectively. Because the imposed charge constraints arises from the EP coupling that invalidates the Born−Oppenheimer approximation,[46] the extent of polaron localization is effectively reflected by the combination coefficients, $C = \{c_i\}$, which can be uniquely determined by matrix diagonalization: $HC = ESC$, where $H$ and $S$ are the Hamiltonian and overlap matrices, respectively, and $E$ is the delocalization energy. In the context of VB theory, the diagonal terms of matrix $H$ are just the electron transfer reorganization energies if the super cell is geometrically optimized with respect to inclusive polaron charge localization on a chosen complex, which is labeled as the pivotal complex with an index of 1. Mathematically, $H_{ii} = E(Q_i,R_1) - E(Q_1,R_1)$, where $Q_i$ indicates the location of the polaron charge and $R_1$ is the optimized geometry of the super cell when the polaron charge is entirely localized on the pivotal complex. As for any off-diagonal term of matrix $H$, it can be considered as the electronic coupling strength between the two corresponding complexes and thus can be evaluated by a method based on orthogonal orbital transformation:[47]

$$H_{ij} = \frac{V_{ij} - S_{ij}(H_{ii} + H_{jj})/2}{1 - S_{ij}^2} \tag{3}$$

where $V_{ij} = \langle\varphi_i|\hat{H}_0|\varphi_i\rangle$ and $S_{ij} = \langle\varphi_i|\varphi_j\rangle$. Rigorously speaking, both $V_{ij}$ and $S_{ij}$ refer to the ones on the dividing plane between two diabatic states. Therefore, prior to the calculations of $V_{ij}$ and $S_{ij}$, a transition state geometry was first optimized under a mixed Hamiltonian: $\hat{H}_{ij} = (1/2)\hat{H}_i + (1/2)\hat{H}_j$, where $i$ and $j$ delineate the locations of the full polaron charge.

Ideally, a complete basis set of our VB approach is formed by exploring all single-site complexes in our super cell. But practically, in light of the limited delocalization of the polaron charge, only the complexes that share atoms with the pivotal complex have to be considered. Moreover, if a pair of complexes does not share any common atom, their coupling is assumed to be zero with regard to the typically rapid decay of electronic coupling strength over distance. Accordingly, 14 and 9 complexes were included in the hole and electron polaron basis sets, respectively, in our calculations. After diagonalizing the corresponding Hamiltonian matrices (see Supporting Information for details) to obtain the combination vector $C$, the extent of polaron charge delocalization was readily determined from the diagonal terms of $C^{\dagger}CS$ and is shown in Figure 3, which also sorts the selected complexes by their

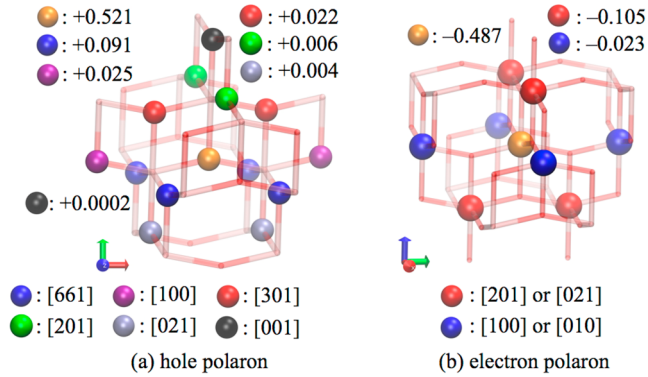


**Figure 3.** Charge delocalization of the hole (a) and electron (b) polarons. A single-site complex is represented by its pivotal atom as a solid sphere. The lattice vectors of the single-site complexes with respect to the pivotal complex (colored orange) are also listed. Please note that a lattice vector of $[n_a n_b n_c]$ is chemically identical to that of $[n_b n_a n_c]$ because the crystal axes of $a$ and $b$ are equivalent in anatase.

geometrical symmetry with respect to their pivotal counterparts. For the hole polaron (Figure 3a), the pivotal complex holds 52.1% of the excess charge while the four [661] complexes (colored blue in Figure 3a) possess 36.6%, the majority of the rest. By contrast, the other nine complexes in total only bear 11.3% of the polaron charge due to their relatively small orbital overlaps and coupling strengths with the pivotal complex. A similar trend was also found in the electron polaron (Figure 3b) wherein the pivotal complex only owns 48.7% of the excess charge while each of the four [201] (or [021]) complexes (colored red in Figure 3b) gains a substantial share of 10.5%, leaving a fairly small sum of 9.2% for the others. A natural indicator of the polaron delocalization extent is the delocalization energy, which is also the lowest eigenvalue of the matrix $S^{-1}H$. It turns out that the delocalization energy for the hole polaron is −4.52 eV, whose magnitude is notably smaller than its electron counterpart of −7.30 eV, suggesting that the electron polaron in bulk anatase $TiO_2$ tends to be more diffuse than the hole polaron. Our hypothesis gains immediate support from the polaron volume calculation, which assumes that the three semiprincipal axes, $\vec{R}_p$, of an ellipsoid polaron are given by

$$\vec{R}_p^{\,2} = \sum_{i=1}^{N} Q_i \vec{r}_i^{\,2} \tag{4}$$

where $Q_i$ is the polaron charge on the $i$ th complex, and $\vec{r}_i$ is the vector connecting the pivotal atoms of the $i$ th complex and its pivotal counterpart. In terms of volume (Figure 4), the electron polaron is nearly twice as large as the hole polaron that clearly marks a stronger EP coupling in hole migration than that in electron diffusion due to the appreciable difference on polaron charge density. Furthermore, the hole polaron (Figure 4a) is rather oblate with two long axes of $R_a = 1.49$ Å and $R_b = 1.16$ Å on the [001] surface and one short axis of $R_c = 0.67$ Å along the surface normal. On the other hand, the electron polaron

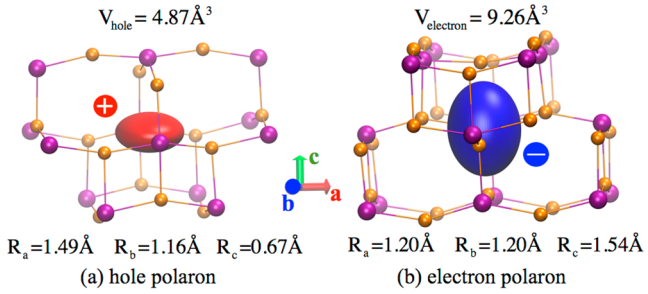


**Figure 4.** Effective size and shape of the hole (a) and electron (b) polarons. The oxygen and titanium atoms are colored orange and purple, respectively.

(Figure 4b) is nearly spherical with a slightly longer $R_c$ of 1.54 Å and two shorter equivalent axes of $R_a = R_b = 1.20$ Å. Because a sphere is known to have the smallest surface-to-volume ratio, the spherical shape of the electron polaron is expected to further facilitate its diffusion compared to its hole counterpart thanks to the diminished polarization effect if one considers the high dielectric constant of anatase, which is usually greater than 30.[48] In our study, the formation of hole polaron results in a lengthening of Ti−O by 0.25 Å along [001], consistent with the bond elongation of 0.29 Å, as reported by a DFT+$U$ study.[14b] Moreover, the closest Ti−O bond in the pivotal electron polaron complex was extended by 0.04 Å, in excellent agreement with 0.05 Å, as revealed by another DFT+$U$ simulation.[14a] Because the hole polaron tends to induce a greater structural change than its electron counterpart in terms of the shortest Ti−O bond length, the EP coupling in the hole polaron is expected to be stronger than that in the electron polaron, leading to a more pronounced charge localization as manifested by Figure 3. According to our definition of charge-weighted ellipsoidal polaron (eq 4), $\vec{r}_{T_i - T_i}$ along [201] and [021] in the electron polaron is 3.02 Å, which is substantially longer than $\vec{r}_{O-O}$ of 2.61 Å along [661] in the hole polaron, a further corroborating evidence for the relative sizes of both polarons. Nevertheless, the number of shared electrons in the distorted pivotal Ti−O bond, which can be estimated from the off-diagonal elements of Mulliken population matrix, turns out to be only 0.18$e$ in both polarons, commonly suggesting a strong ionic bonding character.

In consideration of the notable delocalization characteristics of both polarons, a complex with inclusive polaron charge, i.e., $Q_{hole} = +1$ or $Q_{electron} = -1$, apparently exaggerates the EP coupling. Although the feature of polaron delocalization can be fully captured by using multiple complexes at the expense of CPU cycles and memory consumption, a computationally more efficient way to construct a delocalized polaron using a single complex is to reduce its constrained charge to the value ascertained on the pivotal complex by our VB method. Specifically, $Q_{hole} = +0.521$ or $Q_{electron} = -0.487$. It turns out that the charge delocalization pattern hardly changed when the simple single-complex approach was adopted to replace the multiple-complex definition for a polaron. With the new polaron definitions in our hands, we are in a good position to evaluate the adiabatic activation energy, $\Delta G^*$, along all possible migration directions, which in turn can be used to evaluate the polaron hopping rates according to eq 2. Please note that the polaron migration in anatase must be adiabatic because of the substantial orbital overlap when a polaron hops to one of its adjacent neighbors as illustrated in Figure 4. Consequently, $\Delta G^*$is given by $E(R_{TS}) - E(R_{SP})$, where $E(R_{SP})$ is the energy of an optimized single-complex polaron, and $R_{TS}$ is the optimized transition state whose Hamiltonian is a mixture of those corresponding to the reactant and product polarons: $\hat{H}_{TS} = (1/2)\hat{H}_R + (1/2)\hat{H}_P$. Under the single-phonon approximation, a vibrational energy of $\hbar\omega_0 = 0.11$ $eV$ was also selected as a key parameter in eq 2 to reflect the longitudinal optical vibrational modes in anatase.[14b,49] Once the polaron hopping rate, $k_p$, is determined, we can apply the Einstein relation to calculate its mobility, $\mu$:

$$\mu = \frac{eR^2 n k_p}{k_B T} \tag{5}$$

where $e$ is the elementary charge, $n$ is the number of equivalent polaron accepting sites, and $R$ is the distance between the reactant and product polarons. For the sake of direct comparison with experiments, the polaron mobility was evaluated at 300 and 1300 K.

As listed in Table 1a, the hole migration along the [661] direction is significantly faster than any of the others by at least 3 orders of magnitude at 300 K for its substantially lower $\Delta G^*$ of 0.31 eV. Therefore, the hole polaron mainly diffuses on the [001] surface as manifested by the projection of $\mu$ onto the three lattice axes that yields $\mu_a = \mu_b = 1.27 \times 10^{-5}$ cm$^2$/V·s and $\mu_c = 0.53 \times 10^{-5}$ cm$^2$/V·s. By contrast, the electron migration along [100] (or [001]) is only about 10 times faster than that

**Table 1. Key Migration Properties for Hole (a) and Electron (b) Polarons at 300 K**

| (a) hole polaron | | | | | | |
|---|---|---|---|---|---|---|
| lattice vector | [661] | [301] | [100] | [201] | [021] | [001] |
| $\Delta G^*$ (eV) | 0.31 | 0.47 | 0.69 | 0.55 | 0.55 | 0.65 |
| $k_p$ (s$^{-1}$) | $1.55 \times 10^8$ | $3.47 \times 10^5$ | $6.28 \times 10^1$ | $1.77 \times 10^4$ | $1.77 \times 10^4$ | $2.94 \times 10^2$ |
| $n$ | 4 | 2 | 2 | 2 | 2 | 1 |
| $R$ (Å) | 2.79 | 2.47 | 3.78 | 3.04 | 3.04 | 3.96 |
| $\mu$ (cm$^2$/V·s) | $1.87 \times 10^{-5}$ | $1.63 \times 10^{-8}$ | $6.29 \times 10^{-12}$ | $1.27 \times 10^{-9}$ | $1.27 \times 10^{-9}$ | $1.78 \times 10^{-11}$ |
| (b) electron polaron | | | | | | |
| lattice vector | | [100] | [001] | [201] | [021] | |
| $\Delta G^*$ (eV) | | 0.30 | 0.30 | 0.34 | 0.34 | |
| $k_p$ (s$^{-1}$) | | $2.25 \times 10^8$ | $2.25 \times 10^8$ | $5.37 \times 10^7$ | $5.37 \times 10^7$ | |
| $n$ | | 2 | 2 | 2 | 2 | |
| $R$ (Å) | | 3.78 | 3.78 | 3.04 | 3.04 | |
| $\mu$ (cm$^2$/V·s) | | $2.50 \times 10^{-5}$ | $2.50 \times 10^{-5}$ | $3.80 \times 10^{-6}$ | $3.80 \times 10^{-6}$ | |

**Table 2. Key Migration Properties for Hole (a) and Electron (b) Polarons at 1300 K**

| (a) hole polaron | | | | | | |
|---|---|---|---|---|---|---|
| lattice vector | [661] | [301] | [100] | [201] | [021] | [001] |
| $\Delta G^*$ (eV) | 0.31 | 0.47 | 0.69 | 0.55 | 0.55 | 0.65 |
| $k_p$ ($s^{-1}$) | $1.64 \times 10^{12}$ | $4.02 \times 10^{11}$ | $5.51 \times 10^{10}$ | $2.02 \times 10^{11}$ | $2.02 \times 10^{11}$ | $7.87 \times 10^{10}$ |
| $n$ | 4 | 2 | 2 | 2 | 2 | 1 |
| $R$ (Å) | 2.79 | 2.47 | 3.78 | 3.04 | 3.04 | 3.96 |
| $\mu$ ($cm^2/V{\cdot}s$) | $1.87 \times 10^{-2}$ | $1.63 \times 10^{-3}$ | $1.40 \times 10^{-3}$ | $3.33 \times 10^{-3}$ | $3.33 \times 10^{-3}$ | $1.10 \times 10^{-3}$ |
| (b) electron polaron | | | | | | |
| lattice vector | [100] | [001] | [201] | [021] | | |
| $\Delta G^*$ (eV) | 0.30 | 0.30 | 0.34 | 0.34 | | |
| $k_p$ ($s^{-1}$) | $1.80 \times 10^{8}$ | $1.80 \times 10^{8}$ | $1.29 \times 10^{12}$ | $1.29 \times 10^{12}$ | | |
| $n$ | 2 | 2 | 2 | 2 | | |
| $R$ (Å) | 3.78 | 3.78 | 3.04 | 3.04 | | |
| $\mu$ ($cm^2/V{\cdot}s$) | $9.16 \times 10^{-2}$ | $9.16 \times 10^{-2}$ | $4.24 \times 10^{-2}$ | $4.24 \times 10^{-2}$ | | |

along [201] (or [021]) because of the small difference between their $\Delta G^*$ (i.e., 0.30 eV vs 0.34 eV). Similarly, a strong directional heterogeneity was also observed on electron diffusion as exhibited by $\mu_a = \mu_b = 2.74 \times 10^{-5}$ $cm^2/V{\cdot}s$ and $\mu_c = 0.60 \times 10^{-5}$ $cm^2/V{\cdot}s$. In general, our calculated $\mu_{hole}$ of $1.87 \times 10^{-5}$ $cm^2/V{\cdot}s$ and $\mu_{electron}$ of $3.92 \times 10^{-5}$ $cm^2/V{\cdot}s$ are of the same order of magnitude as the low experimental mobilities of $\sim 10^{-5}$ $cm^2/V{\cdot}s$[50] at room temperature. Moreover, $\mu_{electron}$was found to be more than 2 times as great as $\mu_{hole}$, conforming to the well-known fact that the undoped anatase $TiO_2$ behaves like a lowly doped n-type semiconductor.[15]

When the temperature is increased from 300 to 1300 K, the polaron migration properties undergo drastic change due to the effectively lowered activation barriers. For example, the directional heterogeneity in mobility becomes much less pronounced for both hole and electron polarons, as shown in Table 2. Specifically, the hole migration along the previously predominant [661] direction is only 3−10 times faster than the others, whereas the electron diffusion along [100] (or [001]) is nearly at the same pace as the [201] (or [021]) direction. Again, our calculated $\mu_{electron}$ of $8.98 \times 10^{-2}$ $cm^2/V{\cdot}s$ and $\mu_{hole}$ of $5.48 \times 10^{-2}$ $cm^2/V{\cdot}s$ at 1300 K are perfectly in line with the single-crystal conductivity measurements[2,51] that deduced an electron mobility of $6.7 \times 10^{-2}$ $cm^2/V{\cdot}s$ and a hole mobility of $5.0 \times 10^{-2}$ $cm^2/V{\cdot}s$. Although the polaron migration is greatly facilitated by the increasing temperature, the undoped anatase is expected to eventually lose its n-type characteristics.

Finally, in order to examine the robustness of our VB approach, additional calculations on $\Delta G^*$ along the most probable migration lattice vectors respectively for hole and electron polarons were carried out using the Becke−Lee−Yang−Parr (BLYP) exchange−correlation functional[52] and/or polarized−valence−triple-$\zeta$ (PVTZ) basis set.[44] As shown in Table 3, the values of $\Delta G^*$ only vary by 0.01 eV upon the functional and/or basis set change. Moreover, it is well-known that the Ti 3d electrons are highly correlated, and an onsite Hubbard correction of 7.5 eV is needed to obtain an experimentally consistent band gap for anatase $TiO_2$ if the PBE functional is used, as shown in a DFT+$U$ study.[53] Thus, $\Delta G^*$ was reevaluated with different $U$ values ranging from 6.5 to 8.5 eV, and small variations of ~0.01 eV were again observed (Figure 5). The insensitivity of $\Delta G^*$ to the choice of $U$ can be attributed to two causes. First, in the CDFT framework, the charge localization was primarily imposed by external Hartree potential rather than by onsite Hubbard correction. Second, both the reactant and transition states may suffer from the charge overdelocalization to similar extents, resulting in error cancellation on $\Delta G^*$. Because the Löwdin population analysis was employed in our DFT+$U$ calculations to determine the Ti 3d orbital occupancy, the values of $\Delta G^*$ should be irrelevant to our chosen polarizable basis set.

**Table 3. Comparison on Activation Energy, $\Delta G^*$, Calculated with Different Exchange−Correlation Functionals and Basis Sets[a]**

| lattice vector | hole [661] | electron [100] |
|---|---|---|
| PBE/PVDZ | 0.31 | 0.30 |
| PBE/PVTZ | 0.30 | 0.29 |
| BLYP/PVTZ | 0.30 | 0.29 |

[a]All numbers in the table are in units of eV.

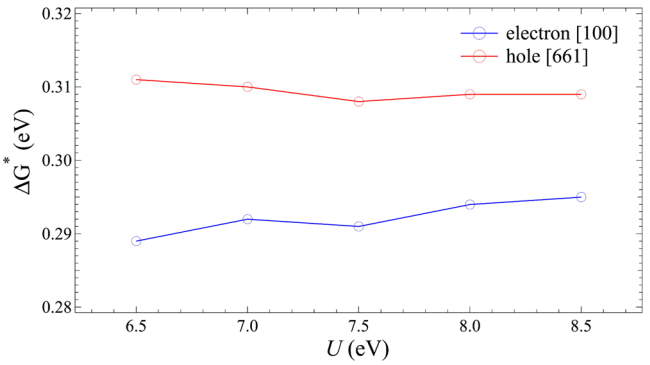


**Figure 5.** $\Delta G^*$ calculated with different onsite Hubbard correction terms, $U$, along the most probable migration lattice vectors respectively for electron and hole polarons.

## 3. CONCLUSIONS

In the present study, a simple yet solid theoretical framework has been established to investigate polaron migration in crystalline materials. Particularly, the size and shape of a polaron are first ascertained by the VB theory, which resorts to CDFT to impose desired charge constraints on the charged complexes before the evaluation of their diabatic energies and coupling strengths. Subsequently, the adiabatic activation energies along all possible migration directions in the crystal lattice are determined by geometry optimization under a

simplified polaron Hamiltonian with a reduced polaron charge as a result of charge delocalization. Finally, the polaron mobility is calculated by the Arrhenius equation with regard to the notable overlap between adjacent polarons. As shown by our simulation results on the hole and electron migration in bulk anatase $TiO_2$, the larger electron polaron is more facile than the smaller hole polaron due to a greater extent of charge delocalization. In addition, compared to the fairly oblate hole polaron, the nearly spherical electron polaron tends to minimize its contact with its highly polarizable surrounding environment. As expected from its shape, the hole polaron exhibits a much stronger directional heterogeneity in migration than its electron counterpart at both 300 and 1300K, wherein our calculated mobilties are in excellent agreement with experimental values. In light of the simplicity, efficiency, and reliability of our VB approach, it will become a valuable tool for modeling polaron migration, a critical process in photocatatlytic water splitting and many other important applications, such as photovoltaic cells,[54] imaging censors,[55] and electrochemical batteries.[56]

## ■ ASSOCIATED CONTENT

### Supporting Information

The Hamiltonian and overlap matrices for electron and hole polarons are listed. The information is available free of charge via the Internet at http://pubs.acs.org.

## ■ AUTHOR INFORMATION


### Corresponding Author

*E-mail: chenhanning@gwu.edu. Fax: 202-994-5873. Phone: 202-992-4492.


### Notes

The authors declare no competing financial interest.

## ■ ACKNOWLEDGMENTS

The research was supported by the start-up grant and the University Facilitating Fund of the George Washington University. Computational resources utilized in this research were provided by the Argonne Leadership Computing Facility (ALCF) at Argonne National Laboratory under Department of Energy contract DE-AC02-06CH11357, by the Extreme Science and Engineering Discovery Environment (XSEDE) at the Texas Advanced Computing Center under National Science Foundation contract TG-CHE130008 and by the Shanghai Supercomputer Center (SSC). We thank Dr. Wei Jiang of ALCF for porting and optimizing CP2K simulation package on IBM BlueGene/Q architecture.

## ■ REFERENCES


(1) Perego, C.; Revel, R.; Durupthy, O.; Cassaignon, S.; Jolivet, J. P. Thermal Stability of $TiO_2$-anatase: Impact of Nanoparticles Morphology on Kinetic Phase Transformation. *Solid State Sci.* **2010**, *12*, 989−995.

(2) Bak, T.; Nowotny, M. K.; Sheppard, L. R.; Nowotny, J. Mobility of Electronic Charge Carriers in Titanium Dioxide. *J. Phys. Chem. C* **2008**, *112*, 12981−12987.

(3) Jalava, J. P. The Use of an Exact Light-Scattering Theory for Spheroidal $TiO_2$ Pigment Particles. *Part. Part. Syst. Charact.* **2006**, *23*, 159−164.

(4) Richards, B. S. Single-material $TiO_2$ Double-layer Antireflection Coatings. *Sol. Energy Mater. Sol. Cells* **2003**, *79*, 369−390.

(5) Popov, A. P.; Zvyagin, A. V.; Lademann, J.; Roberts, M. S.; Sanchez, W.; Priezzhev, A. V.; Myllylä, R. Designing Inorganic Light-Protective Skin Nanotechnology Products. *J. Biomed. Nanotechnol.* **2010**, *6*, 432−451.

(6) Renault, C.; Balland, V.; Martinez-Ferrero, E.; Nicole, L.; Sanchez, C.; Limoges, B. Highly Ordered Transparent Mesoporous $TiO_2$ Thin Films: An Attractive Matrix for Efficient Immobilization and Spectroelectrochemical Characterization of Cytochrome c. *Chem. Commun.* **2009**, *48*, 7494−7496.

(7) Landmann, M.; Rauls, E.; Schmidt, W. G. The Electronic Structure and Optical Response of Rutile, Anatase and Brookite $TiO_2$. *J. Phys.: Condens. Matter* **2012**, *24*, 195503−195508.

(8) Fujishima, A.; Honda, K. Electrochemical Photolysis of Water at a Semiconductor Electrode. *Nature* **1972**, *238*, 37−38.

(9) Smalley, R. E. Future Global Energy Prosperity: The Terawatt Challenge. *MRS Bull.* **2005**, *30*, 412−417.

(10) Park, J. H.; Kim, S.; Bard, A. J. Novel Carbon-Doped $TiO_2$ Nanotube Arrays with High Aspect Ratios for Efficient Solar Water Splitting. *Nano Lett.* **2005**, *6*, 24−28.

(11) Liu, Z.; Hou, W.; Pavaskar, P.; Aykol, M.; Cronin, S. B. Plasmon Resonant Enhancement of Photocatalytic Water Splitting Under Visible Illumination. *Nano Lett.* **2011**, *11*, 1111−1116.

(12) Li, Z.; Yao, C.; Yu, Y.; Cai, Z.; Wang, X. Highly Efficient Capillary Photoelectrochemical Water Splitting Using Cellulose Nanofiber-Templated $TiO_2$ Photoanodes. *Adv. Mater.* **2014**, *26*, 2262−2267.

(13) Ma, X.; Dai, Y.; Guo, M.; Huang, B. Relative Photooxidation and Photoreduction Activities of the {100}, {101}, and {001} Surfaces of Anatase $TiO_2$. *Langmuir* **2013**, *29*, 13647−13654.

(14) (a) Deskins, N. A.; Dupuis, M. Electron Transport via Polaron Hopping in Bulk $TiO_2$: A Density Functional Theory Characterization. *Phys. Rev. B* **2007**, *75*, 195212−195221. (b) Deskins, N. A.; Dupuis, M. Intrinsic Hole Migration Rates in $TiO_2$ from Density Functional Theory. *J. Phys. Chem. C* **2008**, *113*, 346−358.

(15) Warren, D. S.; Shapira, Y.; Kisch, H.; McQuillan, A. J. Apparent Semiconductor Type Reversal in Anatase $TiO_2$ Nanocrystalline Films. *J. Phys. Chem. C* **2007**, *111*, 14286−14289.

(16) Szymanski, P.; El-Sayed, M. Some Recent Developments in Photoelectrochemical Water Splitting Using Nanostructured $TiO_2$: A Short Review. *Theor. Chem. Acc.* **2012**, *131*, 1202−1214.

(17) (a) Deák, P.; Kullgren, J.; Frauenheim, T. Polarons and Oxygen Vacancies at the Surface of Anatase $TiO_2$. *Phys. Status Solidi RRL* **2014**, *8*, 583−586. (b) Gong, X. Q.; Selloni, A.; Batzill, M.; Diebold, U. Steps on Anatase $TiO_2$(101). *Nat. Mater.* **2006**, *5*, 665−670. (c) Di Valentin, C.; Selloni, A. Bulk and Surface Polarons in Photoexcited Anatase $TiO_2$. *J. Phys. Chem. Lett.* **2011**, *2*, 2223−2228.

(18) (a) Yildiz, A.; Iacomi, F.; Mardare, D. Polaron Transport in $TiO_2$ Thin Films. *J. Appl. Phys.* **2010**, *108*, 083701−083708. (b) Sezen, H.; Buchholz, M.; Nefedov, A.; Natzeck, C.; Heissler, S.; Di Valentin, C.; Wöll, C., Probing Electrons in $TiO_2$ Polaronic Trap States by IR-absorption: Evidence for the Existence of Hydrogenic States. *Sci. Rep.* **2014**, *4*, 10.1038/srep03808. (c) Moser, S.; Moreschini, L.; Jaćimović, J.; Barišić, O. S.; Berger, H.; Magrez, A.; Chang, Y. J.; Kim, K. S.; Bostwick, A.; Rotenberg, E.; Forró, L.; Grioni, M. Tunable Polaronic Conduction in Anatase $TiO_2$. *Phys. Rev. Lett.* **2013**, *110*, 196403−196407.

(19) Rosso, K.; Dupuis, M. Electron Transfer in Environmental Systems: A Frontier for Theoretical Chemistry. *Theor. Chem. Acc.* **2006**, *116*, 124−136.

(20) Plata, J. J.; Márquez, A. M.; Sanz, J. F. Electron Mobility via Polaron Hopping in Bulk Ceria: A First-Principles Study. *J. Phys. Chem. C* **2013**, *117*, 14502−14509.

(21) (a) Emin, D.; Holstein, T. Studies of Small-polaron Motion IV. Adiabatic Theory of the Hall Effect. *Ann. Phys.* **1969**, *53*, 439−520. (b) Austin, I. G.; Mott, N. F. Polarons in Crystalline and Non-crystalline Materials. *Adv. Phys.* **2001**, *50*, 757−812.

(22) Perdew, J. P.; Zunger, A. Self-interaction Correction to Density-functional Approximations for Many-electron Systems. *Phys. Rev. B* **1981**, *23*, 5048−5079.

(23) Iordanova, N.; Dupuis, M.; Rosso, K. M. Theoretical Characterization of Charge Transport in Chromia ($\alpha$-$Cr_2O_3$). *J. Chem. Phys.* **2005**, *123*, 074710−074720.
(24) Bezugly, V.; Birkenheuer, U. Multireference Configuration Interaction Treatment of Excited-state Electron Correlation in Periodic Systems: the Band Structure of Trans-polyacetylene. *Chem. Phys. Lett.* **2004**, *399*, 57−61.
(25) Naik, I. K.; Tien, T. Y. Small-polaron Mobility in Non-stoichiometric Cerium Dioxide. *J. Phys. Chem. Solids* **1978**, *39*, 311−315.
(26) Heitler, W.; London, F. Wechselwirkung neutraler Atome und homöopolare Bindung nach der Quantenmechanik. *Z. Physik* **1927**, *44*, 455−472.
(27) Wu, Q.; Van Voorhis, T. Extracting Electron Transfer Coupling Elements from Constrained Density Functional Theory. *J. Chem. Phys.* **2006**, *125*, 164105−164113.
(28) (a) Holstein, T. Studies of Polaron Motion: Part I. The Molecular-crystal Model. *Ann. Phys.* **1959**, *8*, 325−342. (b) Holstein, T. Studies of Polaron Motion: Part II. The "Small" Polaron. *Ann. Phys.* **1959**, *8*, 343−389.
(29) Landau, L. D. Über die Bewegung der Elektronen in Kristallgitter. *Physik Z. Sowjetunion* **1933**, *3*, 644−645.
(30) Hendry, E.; Wang, F.; Shan, J.; Heinz, T. F.; Bonn, M. Electron Transport in $TiO_2$ Probed by THz Time-domain Spectroscopy. *Phys. Rev. B* **2004**, *69*, 081101−081104.
(31) Fivaz, R.; Mooser, E. Electron-Phonon Interaction in Semiconducting Layer Structures. *Phys. Rev.* **1964**, *136*, 833−836.
(32) Fehske, H.; Trugman, S. A. Numerical Solution of the Holstein Polaron Problem. In *Polarons in Advanced Materials*; Alexandrov, A. S., Ed. Springer: Netherlands, 2007; Vol. *103*, pp 393−461.
(33) Brunschwig, B. S.; Logan, J.; Newton, M. D.; Sutin, N. A Semiclassical Treatment of Electron-exchange Reactions. Application to the Hexaaquoiron(II)-hexaaquoiron(III) system. *J. Am. Chem. Soc.* **1980**, *102*, 5798−5809.
(34) Marcus, R. A. Chemical and Electrochemical Electron-Transfer Theory. *Annu. Rev. Phys. Chem.* **1964**, *15*, 155−196.
(35) Truhlar, D. G.; Garrett, B. C. Variational Transition State Theory. *Annu. Rev. Phys. Chem.* **1984**, *35*, 159−189.
(36) (a) Holstein, T. D.; Turkevich, L. A. Field Theory for the One-dimensional Optical Polaron. I. Incorporation of the Goldstone Mode and Interaction with Internal Phonons. *Phys. Rev. B* **1988**, *38*, 1901−1922. (b) Holstein, T. D.; Turkevich, L. A. Field Theory for the One-dimensional Optical polaron. II. Phonon-polaron Scattering. *Phys. Rev. B* **1988**, *38*, 1923−1937.
(37) Munn, R. W.; Silbey, R. Theory of Electronic Transport in Molecular Crystals. II. Zeroth-order States Incorporating Nonlocal Linear Electron−phonon Coupling. *J. Chem. Phys.* **1985**, *83*, 1843−1853.
(38) Michael, D.; Carmen, M. The Peierls−Hubbard Model at Weak Coupling. *J. Phys.: Condens. Matter* **2005**, *17*, 2663−2670.
(39) Berger, T.; Sterrer, M.; Diwald, O.; Knözinger, E.; Panayotov, D.; Thompson, T. L.; Yates, J. T. Light-Induced Charge Separation in Anatase $TiO_2$ Particles. *J. Phys. Chem. B* **2005**, *109*, 6061−6068.
(40) Ahmed, A. Y.; Kandiel, T. A.; Oekermann, T.; Bahnemann, D. Photocatalytic Activities of Different Well-defined Single Crystal $TiO_2$ Surfaces: Anatase versus Rutile. *J. Phys. Chem. Lett.* **2011**, *2*, 2461−2465.
(41) VandeVondele, J.; Krack, M.; Mohamed, F.; Parrinello, M.; Chassaing, T.; Hutter, J. Quickstep: Fast and Accurate Density Functional Calculations Using a Mixed Gaussian and Plane Waves Approach. *Comput. Phys. Commun.* **2005**, *167*, 103−128.
(42) Goedecker, S.; Teter, M.; Hutter, J. Separable Dual-space Gaussian Pseudopotentials. *Phys. Rev. B* **1996**, *54*, 1703−1710.
(43) Perdew, J. P.; Burke, K.; Ernzerhof, M. Generalized Gradient Approximation Made Simple. *Phys. Rev. Lett.* **1996**, *77*, 3865−3868.
(44) Woon, D. E.; Dunning, T. H. Gaussian Basis Sets for Use in Correlated Molecular Calculations. IV. Calculation of Static Electrical Response Properties. *J. Chem. Phys.* **1994**, *100*, 2975−2988.
(45) Blöchl, P. E. Electrostatic Decoupling of Periodic Images of Planewave-expanded Densities and Derived Atomic Point Charges. *J. Chem. Phys.* **1995**, *103*, 7422−7428.
(46) Born, M.; Oppenheimer, R. Zur Quantentheorie der Molekeln. *Annalen der Physik* **1927**, *389*, 457−484.
(47) Farazdel, A.; Dupuis, M.; Clementi, E.; Aviram, A. Electric-field Induced Intramolecular Electron Transfer in Spiro $\pi$-electron Systems and Their Suitability as Molecular Electronic Devices. A Theoretical Study. *J. Am. Chem. Soc.* **1990**, *112*, 4206−4214.
(48) Busani, T.; Devine, R. A. B. Dielectric and Infrared Properties of $TiO_2$ Films Containing Anatase and Rutile. *Semicond. Sci. Technol.* **2005**, *20*, 870−875.
(49) Gonzalez, R. J.; Zallen, R.; Berger, H. Infrared Reflectivity and Lattice Fundamentals in Anatase $TiO_2$. *Phys. Rev. B* **1997**, *55*, 7014−7017.
(50) Dittrich, T.; Lebedev, E. A.; Weidmann, J. Electron Drift Mobility in Porous $TiO_2$ (Anatase). *Phys. Status Solidi A* **1998**, *165*, R5−R6.
(51) Balachandran, U.; Eror, N. G. Electrical Conductivity in Non-stoichiometric Titanium Dioxide at Elevated Temperatures. *J. Mater. Sci.* **1988**, *23*, 2676−2682.
(52) (a) Becke, A. D. Density-functional Exchange-energy Approximation with Correct Asymptotic Behavior. *Phys. Rev. A* **1988**, *38*, 3098−3100. (b) Lee, C.; Yang, W.; Parr, R. G. Development of the Colle-Salvetti Correlation-energy Formula into a Functional of the Electron Density. *Phys. Rev. B* **1988**, *37*, 785−789.
(53) Christopher, E. P.; Feliciano, G. GW Quasiparticle Bandgaps of Anatase $TiO_2$ Starting from DFT+U. *J. Phys.: Condens. Matter* **2012**, *24*, 202201−202205.
(54) Grätzel, M. Dye-sensitized Solar Cells. *J. Photochem. Photobiol. C* **2003**, *4*, 145−153.
(55) Chin, X. Y.; Yin, J.; Wang, Z.; Caironi, M.; Soci, C. Mapping Polarons in Polymer FETs by Charge Modulation Microscopy in the Mid-infrared. *Sci. Rep.* **2014**, *4*, 3626−3631.
(56) Kang, J.; Jung, Y. S.; Wei, S.-H.; Dillon, A. C. Implications of the Formation of Small Polarons in $Li_2O$ for Li-air Batteries. *Phys. Rev. B* **2012**, *85*, 035210−035214.